New Journal of Physics
The open access journal for physics

Population kinetics and M band emission spectra of gold plasmas in non-local thermodynamic equilibrium by using a detailed relativistic configuration approach

Cheng Gao[1], Fengtao Jin[1], Jiaolong Zeng[1,3] and Jianmin Yuan[1,2]

[1] Department of Physics, College of Science, National University of Defense Technology, Changsha 410073, Hunan, People's Republic of China
[2] State Key Laboratory of High Performance Computing, National University of Defense Technology, Changsha 410073, Hunan, People's Republic of China
E-mail: jiaolongzeng@hotmail.com

New Journal of Physics **15** (2013) 015022 (16pp)
Received 31 July 2012
Published 29 January 2013
Online at http://www.njp.org/
doi:10.1088/1367-2630/15/1/015022

Abstract. A collisional-radiative model based on the approach of detailed relativistic configurations is developed, where the complete set of atomic data including photo-excitation, photoionization, electron impact excitation, electron impact ionization and autoionization is calculated, and the data of the inverse processes are obtained by detailed balance. The population distribution is obtained by solving the rate equation under the steady-state condition. The present model is applied to calculate the charge state distribution and M band emission spectra of gold plasmas in non-local thermodynamic equilibrium under a variety of plasma conditions. Comparisons between the present work and experimental results were made and good agreement is found. For the strong transition lines, the intensities predicted by the present model agree with those of experimental spectra within 50%. The present work is useful in analyzing and interpreting experiments as well as in diagnosing the electron temperature in experiments.

[3] Author to whom any correspondence should be addressed.

Contents

1. Introduction

Radiative properties of gold plasmas are of great significance in many research fields such as inertial confinement fusion (ICF) [1, 2]. In indirect driven ICF experiments, the deuterium–tritium target is heated by the x-rays irradiated by laser-produced gold plasmas. For understanding the physics, such as energy deposition and temperature relaxation in the gold hohlraum cavity, it is necessary to predict the correct charge state distribution (CSD) and radiative properties of gold plasmas. For plasmas in local thermodynamic equilibrium (LTE), one can obtain the CSD by solving the Saha–Boltzmann equation [3–5]. However, the plasmas are usually in non-LTE (NLTE) in many ICF processes. In order to calculate the CSD of NLTE plasmas, one needs to solve the rate equation. Based on various approximations, some kinds of models such as detailed level accounting (DLA), detailed configuration accounting (DCA), super-configuration accounting (SCA) and the average atom (AA) model are developed to predict the CSD of NLTE plasmas in recent decades [6–14]. Much effort has been devoted to this field and one can see the reviews in NLTE code comparison workshops [15–19]. For low-Z elements, good agreement is obtained between different models. However, a large discrepancy is found for high-Z elements such as gold, where the mean charge state predicted by different models can spread as large as ten ionization stages [19].

Experimentally, there are a few reports on the measurement of NLTE gold plasmas [20–23]. For example, Foord *et al* [20] obtained the CSD and M band emission spectra of laser-produced gold plasma at $T_e = 2200$ eV and $n_e = 6 \times 10^{20}$ cm^{-3}. Heeter *et al* [23] carried out a 'benchmark' measurement for NLTE gold plasmas in hohlraum where the electron temperature ranges from 800 to 2400 eV and the electron density is near 10^{21} cm^{-3}. These experiments are mainly performed under the condition that the mean charge state of gold plasmas is about 50 (Cu-like) [20–23].

Under the above experimental conditions, gold ions with open N or M shells present a challenge for theoretical modeling. On the one hand, the degeneracy of quantum states is so strong that one should include adequate states in calculations which greatly increase the scale of the matrix in the rate equation. On the other hand, transitions involved by electrons in the d and f shells can produce thousands of millions of transition lines, which bring a great challenge to spectra modeling. Therefore, the detailed models such as DLA are difficult to be applied to predict the CSD of NLTE gold plasmas under these conditions. Instead, the statistical models such as SCA and AA are mainly used to reproduce the CSD of these experiments [8, 12, 13, 24, 25]. However, large discrepancies between experiments and theories are found for both the CSD and the spectra. In the recent 'benchmark' experiment [23], Heeter *et al* simulated the M band

emission spectra by using a hybrid model in which the atomic data are obtained by using the DLA method for lowly excited configurations and UTA for highly excited configurations. To the best of our knowledge, there are no systematic comparisons between the experimental and theoretical results in one unified theoretical framework.

In this work, a collisional-radiative (CR) model implemented by a detailed relativistic configuration approach is developed to calculate CSD and M band emission spectra of NLTE gold plasmas in a variety of plasma conditions. A complete set of atomic data including photoexcitation, photoionization, electron impact excitation, electron impact ionization, autoionization as well as the inverse processes is obtained based on relativistic configurations. The population distribution is obtained by solving the rate equation under the steady-state condition and the M band emission spectra are calculated. Systematic comparisons with the experiments mentioned above are made. This paper is arranged as follows. The theoretical method is introduced in section 2 and the atomic model is described in section 3. In section 4, the CSD and M band emission spectra of NLTE gold plasmas in various plasma conditions are obtained and compared with the experimental results. The conclusion is given in section 5.

2. The theoretical method

In the present CR model, the populations are obtained by solving steady-state rate equations. In the steady-state assumption, the populations of the quantum states (relativistic configurations) are constant, due to the exact balance between the various populating and depopulating atomic processes. For each configuration i, the rate equation can be written as

$$\frac{\mathrm{d}n_i}{\mathrm{d}t} = \sum_{j\neq i}^{N_\mathrm{C}} n_j R_{ji} - \sum_{j\neq i}^{N_\mathrm{C}} n_i R_{ij}, \tag{1}$$

where n_i is the population of configuration i, R_{ij} and R_{ji} represent the rate coefficients which depopulate and populate for the configuration i, respectively, and N_C is the total number of configurations included in the rate equation.

The atomic data including energy of relativistic configurations, transition probabilities, photoionization cross section, electron impact excitation and ionization cross section and autoionization probability are calculated by using the Flexible Atomic Code (FAC) [26]. A fully relativistic approach based on the Dirac equation is used throughout the entire package. The present calculations are carried out based on the relativistic configurations. Once the required atomic data have been obtained, the rate coefficients can be determined. For example, the rate coefficients due to photoionization can be obtained from the corresponding cross section σ_{ij}:

$$\alpha_{ij} = \int_{I/h}^{\infty} \frac{8\pi\nu^2}{c^2} f_\nu \sigma_{ij}\, \mathrm{d}\nu, \tag{2}$$

where I is the ionization potential, ν is the photon frequency and f_ν is the distribution function of photons. Besides, the rate coefficient of the corresponding inverse process, radiative recombination, can be expressed as

$$\beta_{ji} = n_\mathrm{e} \int_0^{\infty} v f(v)(1+f_\nu)\sigma_{ji}^\mathrm{r}\, \mathrm{d}v, \tag{3}$$

where n_e is the electron density, σ_{ji}^r is the cross section of radiative recombination obtained by the detailed balance principle, v is the velocity of the injected electron and $f(v)$ is the electron

distribution function. Here, Maxwellian distribution is used in the present model. The detailed definitions of other rate coefficients can be found in [27].

In the present method, the Stewart–Pyatt model [28] is used to determine the continuum lowering (CL) $\Delta\phi_i$ for ion i caused by screening effects of plasma environments, which is expressed as

$$\Delta\phi_i = \frac{[3(z^*+1)\frac{z_i}{DkT}+1]^{2/3}}{2(z^*+1)}kT, \tag{4}$$

where D is the Debye length, z_i is the charge of ion i and z^* is the mean ionization degree.

The total emission spectrum $j(h\nu)$ is contributed by bound–bound, free–bound and free–free transitions:

$$j(h\nu) = j_{\mathrm{bb}}(h\nu) + j_{\mathrm{fb}}(h\nu) + j_{\mathrm{ff}}(h\nu). \tag{5}$$

The bound–bound contribution can be expressed as

$$j_{\mathrm{bb}}(h\nu) = \sum_{j>i} N_j h\nu A_{ji} S(h\nu), \tag{6}$$

where N_j is the population of the upper state of the transition $j \to i$, and A_{ji} and $S(h\nu)$ are the radiative transition probability and line profile of the transition $j \to i$, respectively. $S(h\nu)$ is taken to be a Voigt profile [4] to account for both electron impact broadening and Doppler broadening.

The free–bound contribution can be written as

$$j_{\mathrm{fb}}(h\nu) = \sum_j n_{\mathrm{e}} N_j h\nu \frac{h\nu - I}{kT_{\mathrm{e}}} \sqrt{\frac{16}{(2\pi m_{\mathrm{e}} kT_{\mathrm{e}})}} \sigma^{\mathrm{r}}(h\nu - I) \mathrm{e}^{-(h\nu-\Delta E)/kT_{\mathrm{e}}}, \tag{7}$$

where n_{e} and T_{e} are the electron density and temperature, respectively. I is the ionization potential and $\sigma^{\mathrm{r}}(h\nu - I)$ is the cross section of radiative recombination. The free–free contribution is

$$j_{\mathrm{ff}}(h\nu) = \frac{2\sqrt{2}}{\sqrt{3\pi}} \alpha\sigma_{\mathrm{T}} c n_{\mathrm{e}} \frac{m_{\mathrm{e}}c^2}{kT_{\mathrm{e}}} g_{\mathrm{ff}} \mathrm{e}^{-h\nu/kT_{\mathrm{e}}} \sum_i n_i Z_i^2, \tag{8}$$

where α is the fine structure constant, σ_{T} is the Thomson scattering cross section, g_{ff} is the Gaunt factor and n_i and Z_i are the ion number and effective nuclear charge of ion with ionization degree i.

3. The atomic model

In this work, gold ions from Au^{39+} to Au^{55+} are included. In the following, Au^{42+} are taken as an example to demonstrate the selection rules of configurations in the present model. We include singly, doubly and triply excited configurations from the ground configuration [Ni]$4s^24p^64d$ as follows: $4s^24p^64f$, $4s^24p^6nl$, $4s^24p^54d^2$, $4s^24p^54d4f$, $4s4p^64d^2$, $4s4p^64d4f$, $4s4p^64dnl$ ($n = 5$–7; $l = 0, 1, 2, \ldots, n-1$), $4s^24p^54f^2$, $4s^24p^54fnl$, $4s4p^64f^2$, $4s4p^64fnl$, $4p^64d^3$, $4p^64d^24f$, $4p^64d^2nl$, $4s^24p^44d^3$, $4s^24p^44d^2nl$, $4s4p^54d^3$, $4s4p^54d^2nl$, $4p^64d4f^2$, $4p^64d4fnl$, $4s^24p^44d4f^2$, $4s^24p^44d4fnl$, $4s4p^54d4f^2$, $4s4p^54d4fnl$ ($n = 5, 6$; $l = 0, 1, 2, \ldots, n-1$), $4s^24p^44f^3$, $4s^24p^34d^4$, $4s^24p^34f^34f$, $4s^24p^34d^24f^2$, $4s^24p^34d4f^3$, $4s^24p^34f^4$, $4s^24p^24d^5$, $4s^24p^24d^44f$, $4s^24p^24d^34f^2$, $4s^24p^24d^24f^3$, $4s^24p^24d4f^4$ and $4s^24p^24f^5$. We also include the configurations with one

electron in M shell excited to N and O shells from the ground, singly and doubly excited configurations mentioned above: $(3)^{17}4s^24p^64d^2$, $(3)^{17}4s^24p^64d4f$, $(3)^{17}4s^24p^64d5l$, $(3)^{17}4s^24p^64f^2$, $(3)^{17}4s^24p^64f5l$, $(3)^{17}4s^24p^54d4f^2$, $(3)^{17}4s^24p^54d4f5l$, $(3)^{17}4s^24p^54f^3$, $(3)^{17}4s^24p^54f^25l$, $(3)^{17}4s^24p^54d^3$, $(3)^{17}4s^24p^54d^24f$, $(3)^{17}4s^24p^64d^2$, $(3)^{17}4s^24p^54d^25l$, $(3)^{17}4s^24p^44d^24f^2$, $(3)^{17}4s^24p^44d^24f5l$, $(3)^{17}4s4p^64d^3$, $(3)^{17}4s4p^64d^24f$, $(3)^{17}4s4p^64d^25l$, $(3)^{17}4s4p^54d^24f^2$, $(3)^{17}4s4p^54d^24f5l$, $(3)^{17}4p^64d^34f$, $(3)^{17}4p^64d^24f^2$, $(3)^{17}4p^64d^24f5l$, $(3)^{17}4s4p^64f^3$, $(3)^{17}4s4p^64f^25l$ ($l = 0, 1, 2, 3, 4$). For convenience, $(3)^{17}$ means the arbitrary occupation for the remaining 17 electrons in M shell which are $3s^23p^63d^9$, $3s^23p^53d^{10}$ and $3s3p^63d^{10}$, respectively. The configurations of other ions are selected according to similar rules and they are not listed here for simplicity.

The present calculations are carried out explicitly based on the detailed relativistic configuration approach. For each ion stage, the atomic data including energy of relativistic configurations, oscillator strength of radiative transitions, cross sections of photoionization, electron impact excitation and ionization and rate of autoionization are obtained for the detailed relativistic configurations formed by the splitting of the selected non-relativistic configurations. The physical effects such as collision cascade are included. The CL due to a plasma environment reduces the total number of relativistic configurations included in the rate equation which is performed in the following way. Again, take Au^{42+} as an example. Once the lowered potential ϕ of Au^{42+} is obtained for a particular plasma condition, the maximum numbers n_{max} and l_{max} (n is the principal quantum number and l is the angular quantum number, respectively) are determined for the Rydberg configurations $4s^24p^6nl$ with energy lower than ϕ. Then, the configurations with the outermost electronic shell nl larger than $n_{max}l_{max}$ are located and the higher excited configurations are removed from the rate equation. The number of relativistic configurations, which is dependent on plasma conditions, is of the order of 10^5. It should be noted that DLA calculation by using these configurations is impractical due to the huge number of fine-structure levels. To solve such a large-scale rate equation, a parallel procedure is developed by calling the ScaLAPACK library [29], which is a library with subroutines for solving the most common problems in numerical linear algebra.

4. Results and discussion

The population distribution is obtained by solving the rate equation under steady-state approximation after the complete set of atomic data is calculated. Table 1 lists the mean charge state of gold plasmas under a variety of electron temperature T_e, electron density n_e and radiative temperature T_r of experiments available in the literature. FLYCHK [13] is an NLTE model where all the atomic data are obtained by a hydrogen-like formula. ABAKO [12] is a similar code to FLYCHK with some improvements. The accuracy of the atomic data obtained by a hydrogen-like formula is discussed in a previous paper [30]. AVERROES [11] is an NLTE model based on the SCA method. RIGEL [21] is an SCA-based CR code which solves for a CSD by using Monte Carlo techniques and MCXSN generates rates for RIGEL based on hydrogenic super-shells. MIST [21] is a low-density tokamak impurity transport code and utilizes the average ion model for the atomic physics rates. In [31], rates of atomic processes are obtained by the AA model. From table 1, one can find that the mean charge state predicted by AVERROES [11] is in good agreement with experimental results. At the same time, AA in [31] always predicted lower values than the corresponding experimental results. The mean charge given by FLYCHK [13] shows agreement with the experimental results at electron temperature of 2200 and 2600 eV,

Table 1. The mean charge state of gold plasmas at a variety of electron temperature T_e, radiative temperature T_r and electron density n_e of experiments available in the literature: a comparison with the experimental and the other theoretical results.

T_e (eV)	T_r (eV)	n_e (10^{20} cm^{-3})	Experiments	This work	Other theories
2500	0	1×10^{-8}	46.8 ± 0.75 [21]	47.13	49.5 [21] (RIGEL/MCXSN)
					42.7 [21] (MIST)
					44.75 [31] (AA)
					47.2 [12] (ABAKO)
					46.4 [11] (AVERROES)
					48.5 [13] (FLYCHK)
2200	0	6	49.3 ± 0.5 [20]	49.11	49.1 [20] (RIGEL)
					49.2 [12] (ABAKO)
					49.6 [11] (AVERROES)
					49.6 [13] (FLYCHK)
					46.79 [31] (AA)
2600	190	14	50.5 ± 1.0 [22]	50.30	50.4 [13] (FLYCHK)
2400	0	6	49.5 ± 0.5 [23]	49.44	
2000	185	6	49.6 ± 0.5 [23]	49.05	
1700	0	7	48.8 ± 0.7 [23]	48.21	
1400	185	10	47.9 ± 1.4 [23]	47.79	
1400	185	9	47.8 ± 1.4 [23]	47.73	
1400	0	10	46.8 ± 1.2 [23]	47.48	
800	185	11	45.3 ± 1.5 [23]	44.52	
800	0	7	42.2 ± 1.2 [23]	43.27	

while it predicts a much larger value than the experimental result at 2500 eV. Among all the theoretical results, it can be seen that the present results are in good agreement with all the experimental results. In the following, we will look into the CSD and M band emission spectra of NLTE gold plasmas in various experimental conditions.

Figure 1 shows the CSD of this work (red) for a gold plasma at $T_e = 2500$ eV and $n_e = 1 \times 10^{12}$ cm^{-3} and the experimental result (black), which is carried out in an electron beam ion trap (EBIT) [21]. Other theoretical results are plotted for comparison. From the inspection of figure 1, one can find that the CSDs of FLYCHK [13] and RIGEL/MCXSN [21] are far away from the experimental result. ABAKO [12] predicts a much narrower width of CSD than the experimental result and a much larger fraction for Au^{47+}. AVERROES [11] predicts a CSD which shifts to the lower ionization stages compared with the experimental results. The present calculation is in good agreement with the experimental result. However, the fraction of highly charged ions such as Au^{50+} and Au^{51+} are a little underestimated.

Figure 2(a) shows the emission spectra of the EBIT gold plasma mentioned above in the photon energy range 3100–3500 eV, which is mainly caused by transitions of $5f \rightarrow 3d$. The calculated spectra are shifted to the lower photon energy range by 6 eV to fit the position of the experimental spectra. The strong emission lines are labeled, where α and β represent transitions of $5f_{7/2} \rightarrow 3d_{5/2}$ and $5f_{5/2} \rightarrow 3d_{3/2}$, respectively. The present spectra are normalized to the intensity of the Au^{47+} α line of the experimental spectra. The emission lines caused by

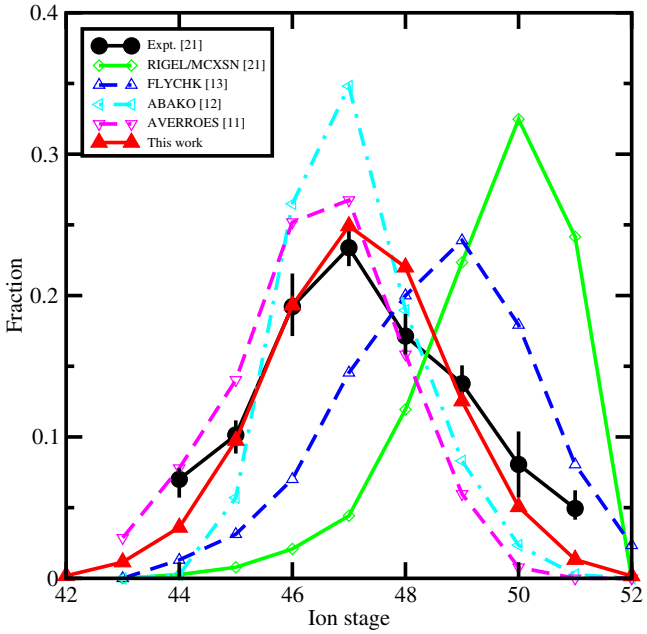

Figure 1. The CSD of a gold plasma at $T_e = 2500\,\text{eV}$ and $n_e = 1 \times 10^{12}\,\text{cm}^{-3}$: a comparison with the experimental and the other theoretical results.

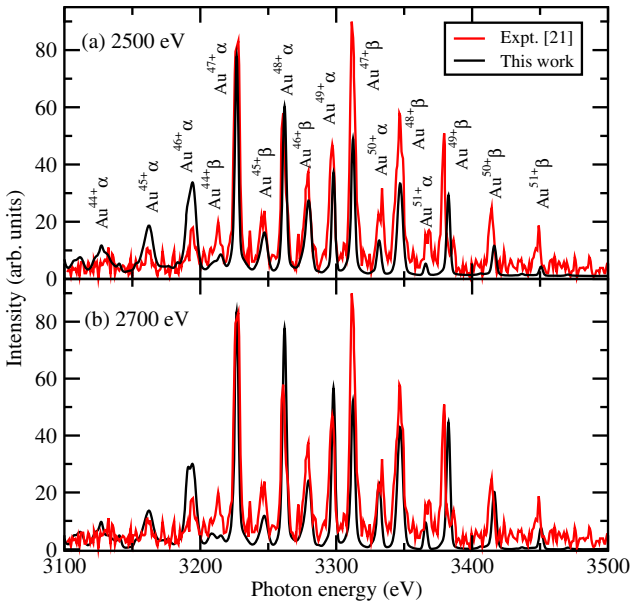

Figure 2. The M band emission spectra of the gold plasma predicted by the present work (black) at electron density $n_e = 1 \times 10^{12}\,\text{cm}^{-3}$ and an electron temperature of (a) 2500 eV and (b) 2700 eV. The experimental spectra are shown in red lines. α and β represent $5f_{7/2} \rightarrow 3d_{5/2}$ and $5f_{5/2} \rightarrow 3d_{3/2}$ transitions, respectively.

$5f_{7/2} \rightarrow 3d_{5/2}$ and $5f_{5/2} \rightarrow 3d_{3/2}$ are separated by about 85 eV due to the spin–orbital splitting. From the inspection of figure 2(a), one can see that the present calculation generally agrees with the experimental spectra. However, the intensity of the emission lines from Au^{49+}–Au^{51+} in the

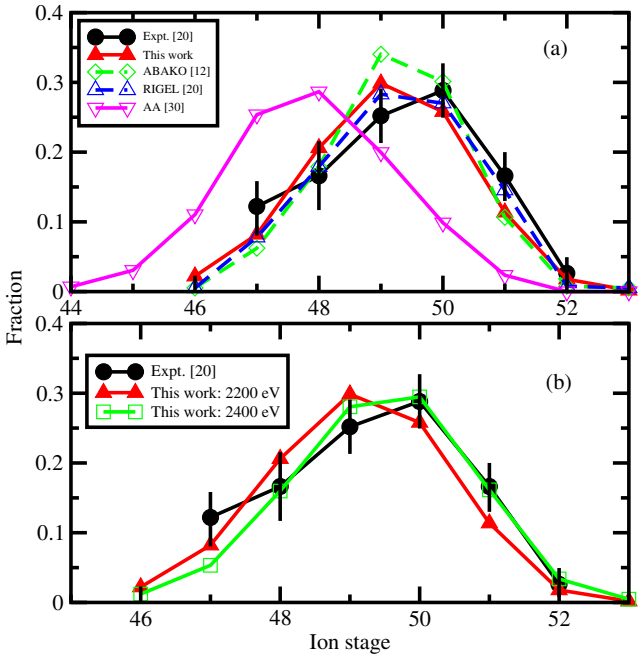

Figure 3. The CSD of a gold plasma at (a) $T_e = 2200\,\text{eV}$ and $n_e = 6 \times 10^{20}\,\text{cm}^{-3}$. In panel (b), the present calculation for $T_e = 2400\,\text{eV}$ and $n_e = 6 \times 10^{20}\,\text{cm}^{-3}$ is plotted (green) and compared with that for $T_e = 2200\,\text{eV}$ (red).

photon energy range 3350–3450 eV predicted by the present work is lower than the experimental result and the largest relative difference is about 50%. The discrepancies are mainly caused by the underestimate for the fraction of these charge states (see figure 1). In panel (b), the emission spectrum of gold plasma at 2700 eV and the same electron density as that in panel (a) ($1 \times 10^{12}\,\text{cm}^{-3}$) are plotted. It can be seen that the agreement between the theoretical and experimental spectra for the lines of Au^{49+}–Au^{51+} is obviously improved, which is mainly caused by the increase of the fraction of Au^{49+}–Au^{51+}: the fraction of Au^{49+}–Au^{51+} at 2500 eV is 12.53, 5.05 and 1.33%, respectively, and the counterparts at 2700 eV are 16.97, 8.30 and 2.66%. The improvement between theory and experiment indicates that there is a temperature gradient of the gold plasma in the experiment.

Figure 3(a) shows the CSD of a laser-produced gold plasma at $T_e = 2200\,\text{eV}$ and $n_e = 6 \times 10^{20}\,\text{cm}^{-3}$ [20]. The CSD predicted by this work, ABAKO [12] and RIGEL [20], are in generally good agreement with the experimental result, while AA [31] predicts a much lower distribution than the experiment. The three theories (this work, ABAKO [12] and RIGEL [20]) predict that Au^{49+} has the largest fraction, while the experiment showed that the most abundant ion stage is Au^{50+}. This can be corrected by increasing the electron temperature within the range of the experimental uncertainty (the uncertainty of electron temperature is 10% according to the experimental report [20]). The CSD of gold plasmas at $T_e = 2400\,\text{eV}$ is calculated and plotted in panel (b). It can be seen that the agreement with the experimental results is improved especially for the Au^{50+}–Au^{53+}.

Figure 4 shows the experimental emission spectra of gold plasma mentioned above (2400 eV) in red lines, where the spectra predicted by the present model are plotted in a solid black line in panel (a) and those predicted by Peyrusse [25] are shown in a dashed black line in

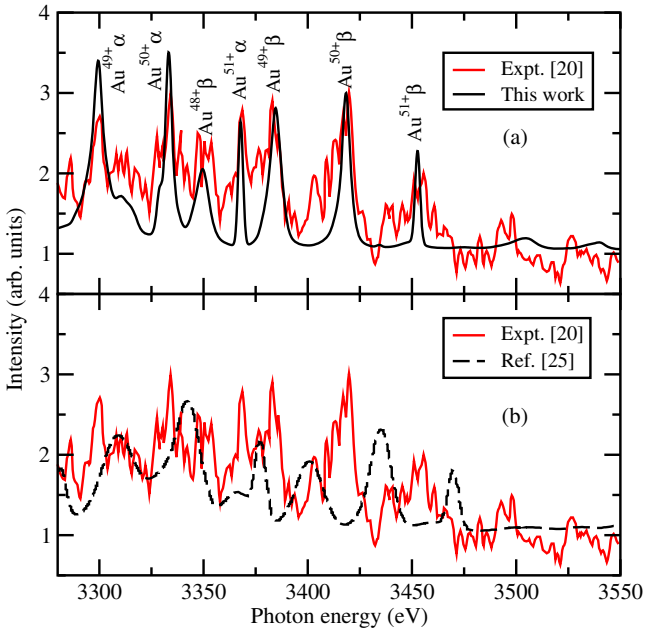

Figure 4. The M band emission spectra of the gold plasma predicted by the present work (black) and experiment (red). α and β represent $5f_{7/2} \rightarrow 3d_{5/2}$ and $5f_{5/2} \rightarrow 3d_{3/2}$ transitions, respectively. The electron temperature is 2400 eV and the density is the same as that in figure 3.

panel (b), respectively. The photon energy is in the range 3250–3550 eV, which is contributed by the 5f → 3d transitions and the transition lines are labeled in panel (a). The present spectra are normalized to the β line ($5f_{5/2} \rightarrow 3d_{3/2}$) of Au^{50+} of the experimental spectra. It can easily be seen that the present results agree much better with the experiment than that predicted by Peyrusse [25], who obtained the spectra by using an SCA method. This indicates that accurate treatment for gold plasmas is important. The relative intensities predicted by the present work such as $Au^{51+}\alpha$ and $Au^{49+}\beta$ are in good agreement with the experiment, yet the intensities of $Au^{49+}\alpha$ and $Au^{50+}\alpha$ are about 25 and 20% larger than the experimental result. Although the present calculation predicts the main emission lines generally well, the satellite lines in the experiment are not predicted well.

We compare the CSD with experiment [22] for a gold plasma at $T_e = 2600$ eV, $T_r = 190$ eV and $n_e = 1.4 \times 10^{21}$ cm^{-3} (figure 5). The predicted mean charge state is 50.3, in good agreement with the experimental value 50.5 ± 1.0. However, there are large discrepancies for the CSD. All theoretical models predict a much lower distribution than the experiment. The experiment gives a large fraction for Au^{52+} which is produced at earlier times when the plasma density is much high and the plasma has not achieved the steady state yet at the time of the measurement [22]. To reproduce the experimental result, the time-dependent calculation is needed and this is not discussed in this paper.

Recently, Heeter *et al* [23] carried out a 'benchmark' measurement for NLTE gold plasmas and the experimental CSDs are shown with black lines in figure 6, which is obtained by the best fitting to the experimental emission spectra. Lines with colors represent the present results. First look at the CSD shown in panel (a) where the electron temperature T_e is 2400 eV and the

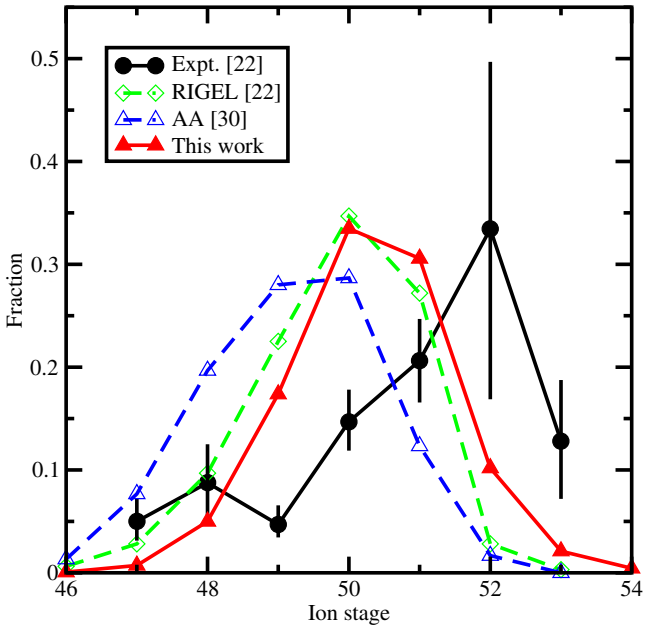

Figure 5. The CSD of a gold plasma at $T_e = 2600\,\text{eV}$, $T_r = 190\,\text{eV}$ and $n_e = 1.4 \times 10^{21}\,\text{cm}^{-3}$.

electron density n_e is $6 \times 10^{20}\,\text{cm}^{-3}$. One can see that the present result agrees well with the experimental result. The experimental emission spectra of the gold plasma under the condition mentioned above in the photon energy range of 3000–4000 eV are shown in red dashed lines in figure 7. The present spectra and theoretical spectra of [23] are plotted in panels (a) and (b), respectively, and they are normalized to the intensity of the experimental line at a photon energy of ∼3420 eV. Heeter *et al* [23] obtained the spectra by using a hybrid model (DLA/UTA) and the atomic data by using FAC code [26]. For a particular ion stage, the configurations formed by single-electron excitation from the ground configuration are treated by the DLA model and others are treated by the UTA model, respectively [23]. The strong emission lines at a photon energy of 3500 and 3700 eV originate from the He α and Ly α lines of impurity potassium in the experiment, which are not included in the present spectra. Similar to the analysis of the emission spectra shown in figure 2, one can identify that the emission lines in the photon energy range of 3100–3200 eV originate from the $4p \rightarrow 3s$ transitions, the lines in 3300–3600 eV are mainly contributed by $5f \rightarrow 3d$ transitions, and lines in 3700–4000 eV are mainly due to $6f \rightarrow 3d$ transitions, respectively. From the inspection of figure 7, one can see that both theoretical spectra are in good agreement with the experimental spectra. However, the agreement is somewhat better for the spectra predicted by the hybrid model [23]. For example, intensities predicted by the present model are about 30% larger than those of the experimental spectra for the lines around photon energy 3300 eV. The intensities predicted by the hybrid model agree with the experiment better than those predicted by the present model, which is mainly caused by the DLA treatment for the lowly excited configurations in the hybrid model. However, one can also find that the width of the lines around photon energy 3300 eV predicted by the hybrid model is larger than that of the experiment.

In figure 6(b), the CSD is given for gold plasma at $T_e = 1400\,\text{eV}$, $n_e = 6 \times 10^{20}\,\text{cm}^{-3}$ and $T_r = 185\,\text{eV}$ [23]. The CSD given by the experiment (black) shows two peaks at Au^{47+} and Au^{50+}

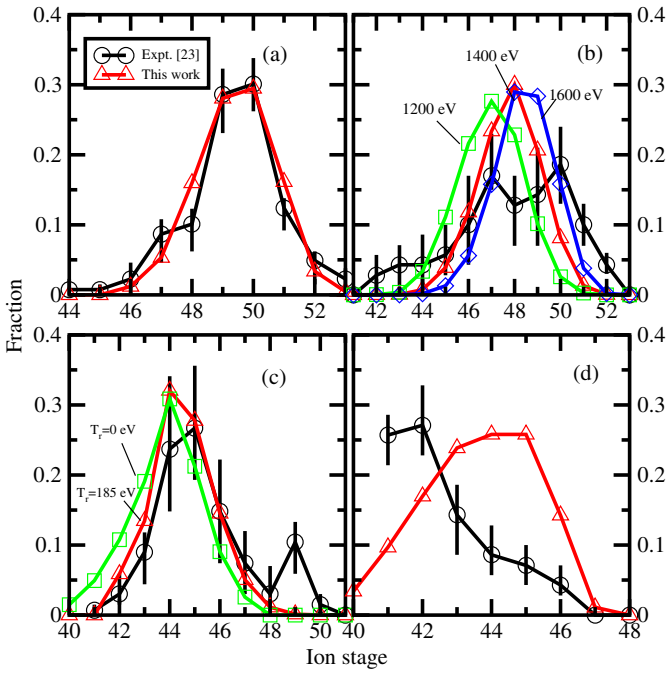

Figure 6. The CSD of gold plasmas of the present work (lines with colors) and experiment (black) at (a) $T_e = 2400\,\text{eV}$, $n_e = 6 \times 10^{20}\,\text{cm}^{-3}$, (b) $T_e = 1400\,\text{eV}$, $n_e = 1 \times 10^{20}\,\text{cm}^{-3}$, (c) $T_e = 800\,\text{eV}$, $n_e = 1.1 \times 10^{21}\,\text{cm}^{-3}$ and (d) $T_e = 800\,\text{eV}$, $n_e = 7 \times 10^{20}\,\text{cm}^{-3}$, respectively. The radiative temperature T_r is 185 eV in panels (b) and (c) and 0 in panels (a) and (d), respectively. In panel (b), the present CSDs at $T_e = 1200$ and 1600 eV are also plotted and in panel (c), the present CSD without radiative field ($T_r = 0$) is plotted.

while the present calculation predicts one peak at Au^{48+} for an electron temperature of 1400 eV (red). The feature of two peaks of the CSD usually indicates that there is a temperature gradient in the experimental plasma. The CSD of the present calculation at an electron temperature of 1200 and 1600 eV is also shown in green and blue lines, respectively. It can be seen that the electron temperature gradient plays an important role in CSD. At an electron temperature of 1200 eV, the peak of CSD shifts to Au^{47+} and at 1600 eV, the most abundant ion is shifted to a higher charge state. Figure 8 shows the present spectra in black lines at an electron temperature of (a) 1200 eV, (b) 1400 eV and (c) 1600 eV, respectively. The experimental spectra are shown in a red dashed line and the theoretical spectra at $T_e = 1400\,\text{eV}$ from [23] are shown in a green line in panel (b). All the theoretical spectra are normalized to the peak of the experimental spectra at a photon energy of 3270 eV. From panel (b), it can be seen that the spectra predicted by the present model agree with that by the hybrid model [23]. The spectra predicted by the hybrid model [23] agree with the experiment better than the present work in the photon energy ranges of 3100–3200 and 3600–3700 eV. However, the intensities of lines in the photon energy range of 3350–3450 eV predicted by both theoretical models are obviously lower than those of the experimental spectra. The discrepancies may be caused by the effect of the temperature gradient on the experimental plasma. From the inspection of figure 8, one can find that the spectra are sensitive to the electron temperature. At 1200 eV, the agreement between the present

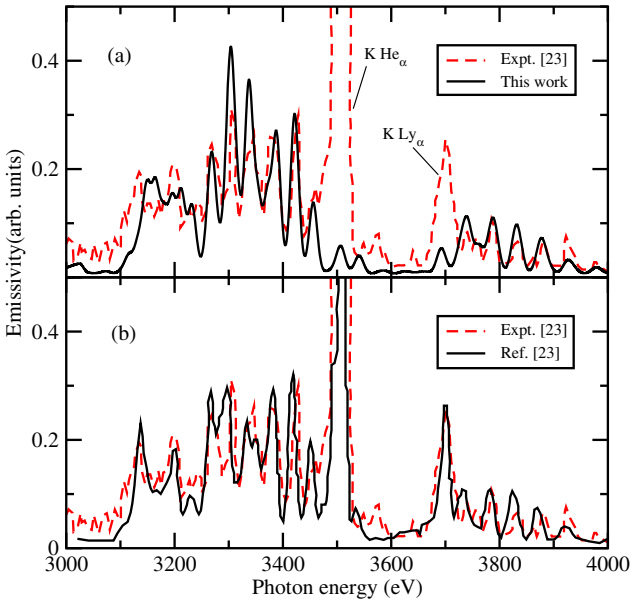

Figure 7. The M band emission spectra of the gold plasma predicted by the present work (black) and experiment (red) at $T_e = 2400\,\text{eV}$ and $n_e = 6 \times 10^{20}\,\text{cm}^{-3}$ (the same as the plasma condition in figure 6(a)).

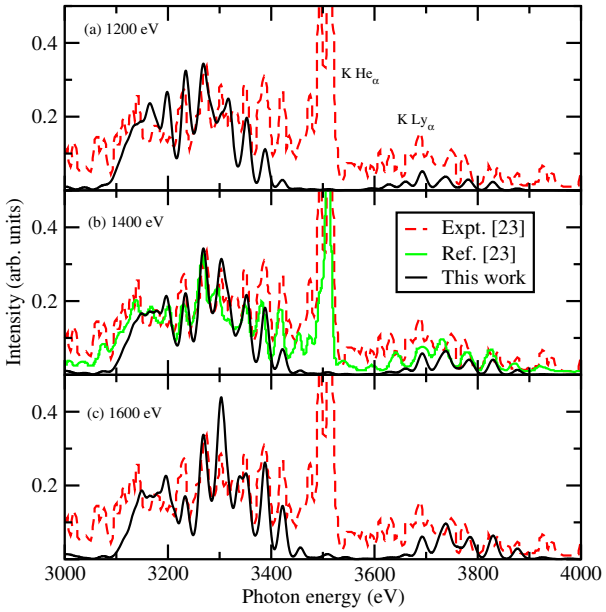

Figure 8. The M band emission spectra of the gold plasma predicted by the present work (black) and experiment (red). The calculated spectra are at a temperature of (a) 1200 eV, (b) 1400 eV and (c) 1600 eV, respectively. The theoretical spectra at an electron temperature of 1400 eV from [23] are shown in a green line in panel (b). The electron density is $6 \times 10^{20}\,\text{cm}^{-3}$ (the same as the plasma condition in figure 6(b)).

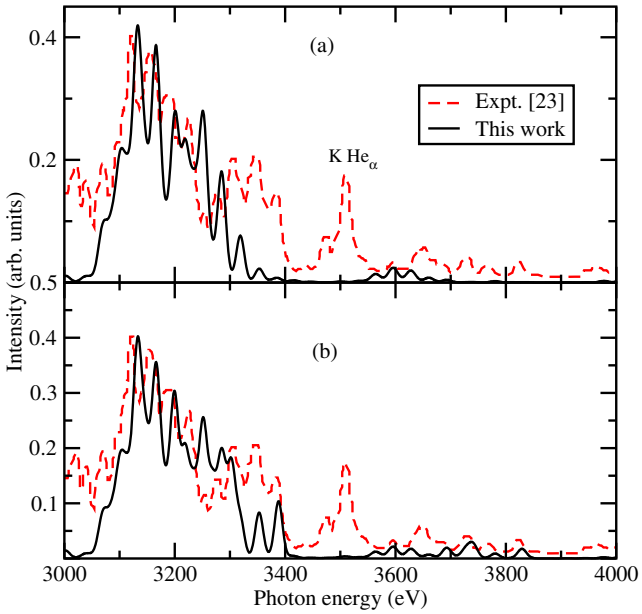

Figure 9. The M band emission spectra of the gold plasma predicted by the present work (black) and experiment (red) at $T_e = 800$ eV, $n_e = 1.1 \times 10^{21}$ cm^{-3} and $T_r = 185$ eV (the same as the plasma condition in figure 6(c)), respectively. In panel (a), the spectrum is calculated with the CSD shown in a red line in figure 6(c). In panel (b), the spectrum is obtained by assuming a fraction of 5% for Au^{48+} and 5% for Au^{49+}, respectively.

spectra and the experiment is good in the photon energy range 3100–3300 eV. However, the intensities predicted by the present model are lower than the experimental spectra in the higher photon energy ranges 3350–3400 and 3600–3900 eV. As the electron temperature increases, the agreement between the present and experimental spectra is getting better in the higher photon energy range and worse in the lower range. At an electron temperature of 1600 eV, the intensities of lines in the photon energy ranges 3350–3400 and 3600–3900 eV agree better with the experiment than those at lower electron temperature. However, the intensity of the line around photon energy 3300 eV is much larger than that of the experiment at lower electron temperature. This indicates that a temperature gradient may exist in the experimental gold plasma.

The CSD of gold plasma shown in figure 6(c) is under the condition of electron temperature 800 eV, electron density 1.1×10^{21} cm^{-3} and radiative temperature 185 eV. The present results with and without radiative field are shown in red triangles and green squares, respectively. The most obvious discrepancy between the present and experimental CSD is that the experiment shows a peak in the tail of CSD (fraction of 10% for Au^{49+}). This is also mainly contributed by other electron temperature ingredients in the experimental plasma. The calculated spectra are shown in figure 9(a) and one can find that the intensity of emission lines in the photon energy ranges of 3300–3400 and 3650–3850 eV is much lower than the experiment. The three peaks in the photon energy of 3300–3400 eV are from the 5f $\rightarrow$ 3d transitions of Au^{48+} and Au^{49+} and the peaks in 3650–3850 eV are from the 6f $\rightarrow$ 3d transitions of Au^{48+} and Au^{49+}, respectively. To reproduce the experimental spectra in these photon energy ranges, one should increase the

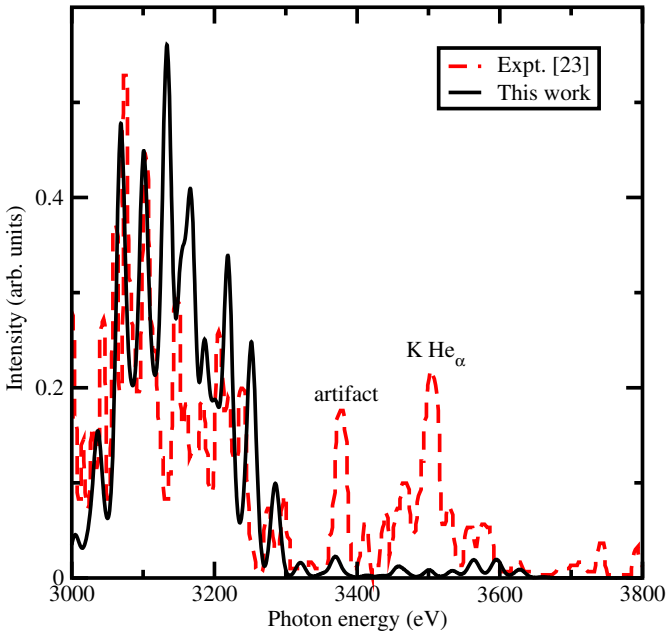

Figure 10. The M band emission spectra of the gold plasma predicted by the present work (black) and experiment (red) at $T_e = 800$ eV, $n_e = 7 \times 10^{20}$ cm^{-3} and $T_r = 0$ (the same as the plasma condition in figure 6(d)). The emission line at photon energy around 3375 eV is an artifact from the experiment [23].

fraction of the two ion stages. In figure 9(b), the calculated spectra are plotted by using an assumed fraction of 5% for Au^{48+} and 5% for Au^{49+}, respectively. It is obvious that the intensity of the peaks in the photon energy ranges of 3300–3400 and 3650–3850 eV is enhanced and the agreement is better, which indicates that there is a temperature gradient in the experimental spectra.

The CSD of the gold plasma at an electron temperature of 800 eV and an electron density of 7×10^{20} cm^{-3} is shown in figure 6(d). A large discrepancy can be seen between the present and experimental results. The main discrepancy for plasma conditions between figures 6(c) and (d) is that the radiative temperature is 185 eV in panel (c) and 0 in panel (d). From the comparison of panels (c) and (d), the experimental result shows that the radiative field can strongly shift the CSD to the lower ionization stages. However, the present calculation does not predict such a strong effect as the experiment does. The corresponding spectra are shown in figure 10, where the emission line at photon energy around 3375 eV is an artifact from the experiment [23]. The intensity of the calculated spectrum in the photon energy range 3100–3200 eV is much higher than the counterparts of the experimental spectra which are mainly contributed by $5f \rightarrow 3d$ transitions of Au^{44+} and Au^{45+}. The discrepancies mainly originate from the overestimated fraction of Au^{44+} and Au^{45+} of the present calculation shown in figure 6(d).

5. Conclusion

In conclusion, a CR model is developed to calculate the population distribution and M band emission spectra of NLTE gold plasmas based on the detailed relativistic configuration

accounting method. A complete set of atomic data such as the energy of relativistic configurations, radiative transition rate, photoionization cross section, electron impact and ionization cross section, and autoionization rate is obtained for Au^{39+}–Au^{55+}. The population distribution of relativistic configurations is obtained by solving the rate equation under the steady-state conditions. Comparisons are made for CSD and M band emission spectra of NLTE gold plasmas between the present calculations and experimental results. Good agreement is found between our calculated mean charge state and all available experiments in the literature at a variety of plasma temperatures and densities. Reasonable agreement is also obtained for the CSD and emission spectra between this work and a few experiments. For most strong transition lines, the intensities predicted by the present model agree with those of experimental spectra within 50%. The present results are helpful in diagnosing the electron temperature in experiments.

Acknowledgments

This work was supported by the National Natural Science Foundation of China under grant numbers 11204376, 11274382 and 11274383 and the Hunan Provincial Innovation Foundation for Postgraduate. Calculations were performed at the Research Center of Supercomputing Application, NUDT.

References

[1] Orlov N Y, Gus'kov S Y, Pikuz S A, Rozanov V B, Shelkovenko T A, Zmitrenko N V and Hammer D A 2007 Theoretical and experimental studies of the radiative properties of hot dense matter for optimizing soft x-ray sources *Laser Part. Beams* **25** 415

[2] Bauche J, Bauche-Arnoult C and Peyrusse O 2006 Effective temperature in hot dense plasmas *J. Quant. Spectrosc. Radiat. Transfer* **99** 55

[3] Iglesias C A, Chen M H, Sonnad V and Wilson B G 2003 A new detailed term accounting opacity code for mid-Z elements: TOPAZ *J. Quant. Spectrosc. Radiat. Transfer* **81** 227

[4] Zeng J and Yuan J 2006 Radiative opacity of gold plasmas studied by a detailed level-accounting method *Phys. Rev.* E **74** 025401

[5] Zeng J 2008 Detailed level accounting investigation on the radiative opacity of gold plasmas at high temperatures *J. Phys. B: At. Mol. Opt. Phys.* **41** 125702

[6] Zeng J, Gang Z and Yuan J 2005 X-ray emission spectra of Ni-like gold ions under coronal plasma condition *Chin. Phys. Lett.* **22** 1972

[7] Itoch M, Yabe T and Kiyokawa S 1987 Collisional-radiative and average-ion hybrid models for atomic processes in high-Z plasmas *Phys. Rev.* A **35** 233

[8] Fontes C J, Abdallah J Jr, Clark R E H and Kilcrease D P 2000 Non-LTE modeling of gold plasmas *J. Quant. Spectrosc. Radiat. Transfer* **65** 223

[9] Abdallah J Jr and Sherrill M E 2008 The reduced detailed configuration accounting (RDCA) model for NLTE plasma calculations *High Energy Density Phys.* **4** 124

[10] Bar-Shalom A, Oreg J and Klapisch M 1997 Non-LTE superconfiguration collisional-radiative model *J. Quant. Spectrosc. Radiat. Transfer* **58** 427

[11] Peyrusse O, Bauche-Arnoult C and Bauche J 2005 Calculation of the charge state distribution of a highly ionized coronal Au plasma *J. Phys. B: At. Mol. Opt. Phys.* **38** L137

[12] Florido R, Rodríguez R, Gil J M, Rubiano J G, Martel P, Mínguez E and Mancini R C 2009 Modeling of population kinetics of plasmas that are not in local thermodynamic equilibrium using a versatile collisional-radiative model based on analytical rates *Phys. Rev.* E **80** 056402

[13] Chung H K and Lee R W 2009 FLYCHK: generalized population kinetics and spectral model for rapid spectroscopic analysis for all elements *High Energy Density Phys.* **5** 1
[14] Gao C and Zeng J 2011 Modeling the population kinetics of NLTE plasmas based on approximations of nonrelativistic configurations *Phys. Scr.* **T144** 014037
[15] Lee R W, Nash J K and Ralchenko Yu 1997 Review of the NLTE kinetics code workshop *J. Quant. Spectrosc. Radiat. Transfer* **58** 737
[16] Bowen C, Decoster A, Fontes C J, Fournier K B, Peyrusse O and Ralchenko Yu V 2003 Review of the NLTE emissivities code comparison virtual workshop *J. Quant. Spectrosc. Radiat. Transfer* **81** 71
[17] Bowen C, Lee R W and Ralchenko Yu 2006 Comparing plasma population kinetics codes: review of the NLTE-3 kinetics workshop *J. Quant. Spectrosc. Radiat. Transfer* **99** 102
[18] Rubiano J G, Flordo R, Bowen C, Lee R W and Ralchenko Yu 2007 Review of the 4th NLTE code comparison workshop *High Energy Density Phys.* **3** 225
[19] Fontes C J, Abdallah J Jr, Bowen C, Lee R W and Ralchenko Yu 2009 Review of the NLTE-5 kinetics workshop *High Energy Density Phys.* **5** 15
[20] Foord M E *et al* 2000 Ionization processes and charge-state distribution in a highly ionized high-Z laser-produced plasma *Phys. Rev. Lett.* **85** 992
[21] Wong K L, May M J, Beiersdorfer P, Fournier K B, Wilson B, Brown G V, Springer P, Neill P A and Harris C L 2003 Determination of the charge state distribution of a highly ionized coronal Au plasma *Phys. Rev. Lett.* **90** 235001
[22] Glenzer S H, Fournier K B, Wilson B G, Lee R W and Suter L J 2001 Ionization balance in inertial confinement fusion hohlraums *Phys. Rev. Lett.* **87** 045002
[23] Heeter R F *et al* 2007 Benchmark measurements of the ionization balance on non-local-thermodynamic-equilibrium gold plasmas *Phys. Rev. Lett.* **99** 195001
[24] Foord M E, Glenzer S H, Thoe R S, Wong K L, Fournier K B, Albritton J R, Wilson B G and Springer P T 2000 Accurate determination of the charge state distribution in a well characterized highly ionized Au plasma *J. Quant. Spectrosc. Radiat. Transfer* **65** 231
[25] Peyrusse O 2001 On the superconfiguration approach to model NLTE plasma emission *J. Quant. Spectrosc. Radiat. Transfer* **71** 571
[26] Gu M F 2003 Indirect X-ray line-formation processes in iron L shell ions *Astrophys. J.* **582** 1241
[27] Rose S J 2009 The effect of a radiation field on excitation and ionisation in non-LTE high energy density plasmas *High Energy Density Phys.* **5** 23
[28] Stewart J C and Pyatt K D Jr 1966 Lowering of ionization potentials in plasmas *Astrophys. J.* **144** 1203
[29] Blackford L S *et al* 1997 *ScaLAPACK Users' Guide* (Philadelphia, PA: Society for Industrial and Applied Mathematics)
[30] Gao C and Zeng J 2010 Validity of analytical formulas for autoionization and dielectronic capture rates used in collisional-radiative models *Phys. Rev.* A **82** 062515
[31] Wu Z Q, Han G X, Yan J and Pang J Q 2004 A kinetic model for non-local thermodynamic equilibrium plasmas *J. Quant. Spectrosc. Radiat. Transfer* **87** 367